

Intragroup diffuse light in compact groups of galaxies II. HCG 15, 35 and 51

C. Da Rocha^{1,2,3} [★], B. L. Ziegler^{1,2} [†] and C. Mendes de Oliveira⁴ [‡]

¹*European Southern Observatory, Karl-Schwarzschild-Str. 2, 85748 Garching, Germany*

²*Institut für Astrophysik, Friedrich-Hund-Platz 1, 37077 Göttingen, Germany*

³*Divisão de Astrofísica, Instituto Nacional de Pesquisas Espaciais (INPE/MCT)*

Av. dos Astronautas 1758, 12227-010, São José dos Campos – SP, Brazil

⁴*Instituto de Astronomia, Geofísica e Ciências Atmosféricas, Universidade de São Paulo,*

Rua do Matão 1226, Cidade Universitária, 05508-900, São Paulo – SP, Brazil

ABSTRACT

This continuing study of intragroup light in compact groups of galaxies aims to establish new constraints to models of formation and evolution of galaxy groups, specially of compact groups, which are a key part in the evolution of larger structures, such as clusters. In this paper we present three additional groups (HCG 15, 35 and 51) using deep wide field *B* and *R* band images observed with the LAICA camera at the 3.5m telescope at the Calar Alto observatory (CAHA). This instrument provides us with very stable flatfielding, a mandatory condition for reliably measuring intragroup diffuse light. The images were analyzed with the OV_WAV package, a wavelet technique that allows us to uncover the intragroup component in an unprecedented way. We have detected that 19, 15 and 26% of the total light of HCG 15, 35 and 51, respectively, is in the diffuse component, with colours that are compatible with old stellar populations and with mean surface brightness that can be as low as 28.4 B mag arcsec^{−2}. Dynamical masses, crossing times and mass to light ratios were recalculated using the new group parameters. Also tidal features were analyzed using the wavelet technique.

Key words: dark matter — galaxies: clusters: general — galaxies: evolution — galaxies: interactions — intergalactic medium

1 INTRODUCTION

Matter can be stripped from galaxies during interaction episodes and form tidal debris (tails, shells and bridges), which, in a dense environment such as a cluster or a group, will be partially re-absorbed by the individual systems and partially dispersed by the cluster tides combined with ram pressure stripping from the hot intracluster medium on a quick timescale. This dispersed matter will settle into the cluster potential, forming a very faint component of intracluster diffuse light (ICL) (Mihos 2004).

This faint component was first observed by Zwicky (1951) in the Coma cluster and has been observed in several other clusters and groups since then and also studied through simulations and theoretical work (see Vílchez-Gómez 1999; Da Rocha & Mendes de Oliveira 2005, for a recent literature review). This component can be used to study the dynamical evolution of structures in a direct

way, since it is related to past galaxy encounters and history of accretion onto the system (Dressler 1984), it then works as an evolutionary clock and it is sensitive to the dark matter distribution, that has a direct effect on the amount of stripped matter. However, the correlations between the properties of the intracluster light and the cluster properties are still not well defined given the large uncertainties and the few studies in this area.

More recent simulations (Rudick, Mihos, & McBride 2006) show the evolution of the ICL with time. A large fraction of the observed evolution in their simulations happens still inside of groups of galaxies that will subsequently be accreted by the cluster afterwards. This shows that the pre-processing of the galaxies and of the intergalactic medium, still in the group environment, strongly influences the properties of the resulting clusters. Murante et al. (2007) also points out that the group dynamical history, previous to the accretion by the cluster, is important and may be the reason for the lack of correlation between the cluster dynamical history and the ICL fraction. The simulations of Murante et al. (2004, 2007) also present a correlation of the ICL with cluster total mass. These authors show that the

[★] E-mail: cdarocha@eso.org

[†] E-mail: bziegler@eso.org

[‡] E-mail: oliveira@astro.iag.usp.br

ICL component has no preferential redshift to start forming, but 70% of it is formed after $z \sim 1$ and its stars would have the same origin as the Brightest Cluster Galaxy's (BCG), at least for $R < 0.5R_{vir}$.

Purcell, Bullock, & Zentner (2007) show that the “halo” on cluster scale (where the ICL would be considered as the cluster halo) originates in massive satellites ($10^{11} M_{\odot}$) while on galaxy scale the halo originates in small mass satellites ($10^{8.5} M_{\odot}$), on the other hand no correlation between the ICL and the total mass of the cluster was found. Conroy, Wechsler, & Kravtsov (2007) results agree with observations, where 80% of the stripped stars are placed in the ICL component and the other 20% settles in the BCG, also showing the parallel evolution of the ICL and the BCG. According to the simulations of Monaco et al. (2006), the ICL has also implications on the low evolution of the high-end of the galaxy mass function ($10^{11} M_{\odot}$) since $z \sim 1$, what is a problem for models of galaxy formation in Λ CDM. That can be solved with the stripping of about 20% of the total stellar mass.

On the observational side, in an analysis with stacked images of clusters in the SDSS (Sloan Digital Sky Survey), Zibetti et al. (2005) and Zibetti (2007) found that the ICL tends to align with the BCG, so that radial orbits would be favored. They also found that clusters with “faint-BCGs” ($M_{r,0} > -22.85$), present a suppression of the ICL that has no correlation with cluster richness. Covone et al. (2006) find that the ICL and the BCG are aligned in Abell 2667 and also the X-Ray component presents the same behaviour. The deep photometric study of Seigar, Graham, & Jerjen (2007) shows that the outer part of the BCG surface brightness profile, which would be associated to the ICL, is better described by an Exponential profile, rather than the usual de Vaucouleurs profile.

Recent studies (Krick & Bernstein 2007) show an anti-correlation between ICL fraction and total cluster mass (also shown by Gonzalez, Zaritsky, & Zabludoff 2007), opposite prediction to the expectation by simulations and an expected correlation, even though weak, between the ICL fraction and the redshift.

On group scale, simulations of isolated groups (Sommer-Larsen 2006) show that the intragroup light component (IGL) increases with time showing its “dynamical clock nature” and that these structures evolve to the so called “fossil groups” (Ponman et al. 1994). Fossil groups are groups in which the magnitude difference between the first and the second-ranked galaxies is larger than 2 magnitudes and the X-Ray halo is extended and has a luminosity higher than $10^{42} h_{50}^{-2} \text{ erg s}^{-1}$ (Jones et al. 2003). By construction of the sample, where all the galaxies should be in a range of three magnitudes, this kind of structure is avoided in the Hickson Compact Groups catalogue (Hickson 1982).

The more recent results from observations and simulations are showing that the evolution of groups of galaxies have significant influence on the evolution of clusters of galaxies. Therefore, understanding the evolution of groups holds the key to explain several effects we are trying to understand in the present time. Our focus on this topic is the study of compact groups of galaxies, and, as in Da Rocha & Mendes de Oliveira (2005), we bring additional data with the determination of the IGL in three new groups.

In our previous work, we studied three compact groups from the Hickson catalogue (Hickson 1982). We have found that the fraction of the total B band (and R band) light in the IGL component is $46 \pm 8\%$ ($33 \pm 6\%$) for HCG 79, $11 \pm 6\%$ ($12 \pm 2\%$) for HCG 95 and there was no IGL detection for HCG 88. We quote here the new error estimates for the IGL light fraction for these groups. The new error estimates are based on new simulations of detection of IGL with the OV_WAV, that cover a larger range in signal to noise ratio. These groups were separated in categories (initial, intermediary and advances stage of evolution) according to their stage of dynamical evolution.

Compact groups of galaxies are formed by three to seven galaxies separated by distances of the order of the galactic diameter (high projected densities) and with a low velocity dispersion ($\sim 200 \text{ km s}^{-1}$, Hickson et al. 1992). In this environment the stripping of material from the galaxies due to interactions, that may give origin to the IGL component, should be a frequent and efficient process. The previous studies of this component in compact groups using photographic plates were only partially successful (Rose 1979; Pildis, Bregman, & Schombert 1995; Sulentic & Lorre 1983; Moles, Marquez, & Sulentic 1998) and only using CCDs a more accurate detection was possible (Nishiura et al. 2000a; White et al. 2003).

Section 2 presents a description of the studied groups HCG 15, 35 and 51. In § 3 the observational data and the reduction procedures applied to the data are presented. In section 4 we present the analysis of the data and results. A discussion and summary are presented in § 5, where we put together the results from the last paper and this one to discuss the evolution of groups. Throughout this work we use $H_0 = 70 \text{ km s}^{-1} \text{ Mpc}^{-1}$, $\Omega_M = 0.3$, $\Omega_{\Lambda} = 0.7$.

2 THE SAMPLE

In this work we studied three more groups from the Hickson Compact Groups catalogue (HCG – Hickson 1982), selected based on X-ray detection (Ponman et al. 1996) and on angular size. The characteristics of the studied groups in this work: HCG 15, 35 and 51, are presented below.

2.1 HCG 15

HCG 15 was originally classified as a sextet of galaxies (Hickson 1982), composed of 3 late-type and 3 early-type galaxies. Hickson et al. (1992) show that all the 6 galaxies have concordant radial velocities (inside $\pm 1000 \text{ km s}^{-1}$ of the median group velocity) with a mean recession velocity of 6832 km s^{-1} (99.3 Mpc). A more recent measurement shows that the elliptical galaxy HCG 15C has a recession velocity of $9687 \pm 22 \text{ km s}^{-1}$ (galaxy UGC 01620 in the Updated Zwicky Catalog - UZC, Falco et al. 1999), that puts this galaxy as an interloper in the group.

We will perform the analysis of this group for the two possible configurations (sextet and quintet, excluding HCG 15C from the group), in order to test which one is compatible with the stage of dynamical evolution of the group.

According to Mendes de Oliveira & Hickson (1994) four of the six galaxies of this group present signs of interaction. The spiral galaxy HCG 15A presents weak

radio emission, the elliptical galaxy HCG 15B shows a dust lane, HCG 15D, also an elliptical, has non-centric isophotes and weak radio emission and the Sbc HCG 15F presents a clear disturbed morphology. This group was detected in X-rays by ROSAT but so far off-axis that it is not possible to distinguish between intragroup and individual galaxies emission (Mulchaey et al. 2003) and the total X-ray luminosity is $\log L_X = 42.12 \text{ erg s}^{-1}$ (Osmond & Ponman 2004). This group presents an HI deficiency of 76% (Verdes-Montenegro et al. 2001) when compared to the expected amount of HI, considering the member galaxies morphological types and luminosities. The total HI of the groups was estimated based on the sextet configuration. The scenario where HCG 15C is a distant galaxy projected onto the group would explain why the galaxy in the center of the group does not present signs of interaction.

The general properties of HCG 15 are presented in table 1.

2.2 HCG 35

HCG 35 is also a sextet (Hickson 1982) dominated by early-type galaxies (5 early-type and 1 late-type), that has a mean recession velocity of 16252 km s^{-1} (241.7 Mpc).

In this group, only HCG 35A was identified with possible signs of interaction, an S0 galaxy showing weak emission lines that extend beyond the nucleus (Mendes de Oliveira & Hickson 1994). It has ROSAT X-ray detection but, as it is also the case of HCG 15, observations do not allow the distinction between intragroup and individual galaxies emission (Mulchaey et al. 2003). Its total X-ray luminosity is $\log L_X = 42.06 \text{ erg s}^{-1}$ (Ponman et al. 1996). This group has an HI overabundance of about 29% with respect to its total expected HI content (Verdes-Montenegro et al. 2001).

General properties of HCG 35 can be seen in table 1.

2.3 HCG 51

This group also presents a “membership issue”. Originally classified as a sextet of galaxies (Hickson 1982), HCG 51C’s radial velocity is $\sim 1200 \text{ km s}^{-1}$ above the group’s median velocity, and therefore it was excluded from the group by Hickson et al. (1992). On the other hand, as explained by these authors, $\pm 1000 \text{ km s}^{-1}$ is an arbitrary threshold, so we decided to analyze both possibilities.

This group is dominated by an E1 galaxy and has 2 late-type and 4 early-type galaxies and HCG 51C is an S0 galaxy. The mean recession velocity of this group is 7924 km s^{-1} (112.6 Mpc), in the quintet configuration.

The only interaction sign identified by Mendes de Oliveira & Hickson (1994) in this group was a faint disk in the center of the elliptical galaxy HCG 51E, even though a very low surface brightness jet-like structure connecting HCG 51A and HCG 51E could be identified in our analysis (see below) and can be related to the origin of the faint disk. The total X-ray luminosity of this group is $\log L_X = 42.70 \text{ erg s}^{-1}$ (Ponman et al. 1996). The HI deficiency compared to the expected HI content is 69% (Verdes-Montenegro et al. 2001), estimated for the quintet configuration.

Table 1. General properties of the observed groups.

	HCG 15	HCG 35	HCG 51
RA	02 ^h 07 ^m 39 ^s 0	08 ^h 45 ^m 19 ^s 5	11 ^h 22 ^m 20 ^s 9
DEC	+02°08′18″	+44°31′18″	+24°17′35″
V_{Rad} (km s ^{−1})	6753/6832*	16252	7728/7924*
Distance (Mpc)	98.2/99.3*	232.2	112.6/115.5*
$(m - M)_V$	35.0	36.9	35.3
Vel. Disp. (km s ^{−1})	471/462*	348	265/535*
Mean. Sep. (kpc)	118/110*	77	86/88*
Num. Gal.	5/6*	6	5/6*

* Values presented for HCG 15 and HCG 51 are given for the quintet and sextet configurations, respectively.

Velocity dispersions were calculated using the correction for the velocity measurements errors described by Danese et al. (1980).

The general properties of HCG 51, as for the other studied groups are summarized in table 1.

3 OBSERVATIONS AND DATA REDUCTION

3.1 Observational data

The studied groups were observed with the wide-field camera LAICA (Large Area Imager for Calar Alto) at the prime focus of the 3.5m telescope of the Calar Alto observatory (CAHA – Centro Astronómico Hispano Alemán). Deep images were obtained in the *B* and *R* bands in December 2003, in non photometric nights, but with sub-arcsecond seeing (from 0.6 to 1.0), with exposure times ranging between 8250 and 12000 seconds in *B* and 3500 and 4000 seconds in *R*. The observational information is summarized in table 2.

The camera LAICA is composed of an array of 2×2 CCDs. Each CCD has $4k \times 4k$ pixels covering a field of view of 15.36×15.36 . CCDs are separated by 13.64, about the size of one CCD, so that the usual observational procedure encompasses 4 pointings shifted by one CCD length, resulting in a field of view of about one degree, covered in 16 separated images. The camera has a pixel size of $0.225''$, and our observations were performed with a 2×2 binning, resulting in pixels of $0.45''$.

Since compact groups of galaxies have a small angular size, each of the observed groups could be fit in one single CCD. This gave us the good advantage of needing only one single pointing per group, not the usual four-pointings procedure. While a group is placed in one single CCD, the other 3 CCDs of the camera were used to observe blank neighboring regions of the sky, thus producing “night sky flats”. By placing each group in a different CCD we obtained a complete set of observed science frames with groups and the corresponding night sky flats with exposure times of the same order. Since flatfielding is a key issue in the study of large scale low surface brightness structures, this observational strategy was very well suited and saved a considerable amount of telescope time. Individual exposures were dithered to correct for CCD defects and cosmic rays.

3.2 Data reduction

The basic data reduction was performed using IRAF¹. One problem encountered was that each CCD of the camera has

Table 2. Observational data.

Group	Band	Exp. (Sec.)	Seeing
HCG 15	B	11250 (15×750)	0''8
	R	4000 (16×250)	0''6
HCG 35	B	12000 (16×750)	0''9
	R	3500 (14×250)	1''0
HCG 51	B	8250 (11×750)	0''9
	R	4000 (16×250)	1''0

a four-port readout, that could affect our analysis that requires stable sky levels. After performing the BIAS and flat-field corrections the difference in the level of each quadrant of the CCD did not disappeared. For this reason we treated each quadrant as a separate image and made a “sky level matching” at the end of the basic data reduction.

As mentioned before, due to our observational strategy, we have two types of images: science images, which are the “on-group” ones, and night sky flats, which are the other three “off-group” images, in each exposure. Each science and sky flat image was cut in four quadrants and the BIAS correction was applied to each of the new “quadrant images”. Due to the non photometric conditions, some of the “off-group” images presented sky patterns and could not be used to produce the night sky flatfields. Those sky patterns were sometimes also present in the “on-group” images which could not be corrected by the flatfields and could not be used to produce our final image. After selecting the useful images, a combination of night sky flat, to correct for the large scale CCD response and for CCD illumination, and twilight flat, to correct for the individual pixel sensitivity was applied to the science frames. The quadrants were rejoined in a single image with matched sky levels. The sky matching consists in measuring the difference in sky level along both sides of the matching region and correcting the sky level by a constant, so that no sky level difference is left and no step-like structure is present in the image. This correction was at the order of a few counts, while the sky level is of the order of some thousands of counts. However, this small variation would have an important effect in our analysis. Images were registered and combined producing a final image for each group in each filter.

Since the nights when the data were taken were not photometric, we need to calibrate our images by comparing them to published data by Mendes de Oliveira (1992). But because the Mendes de Oliveira (1992) image sizes are quite small ($2''.2 \times 3''.5$), we could not measure a useful number of stars in common for the calibration (the few ones available in these fields were, in most cases, saturated in our images). We, therefore, decided to use the calibrated profiles of the galaxies themselves, in order to find the zero points for the images. We matched the instrumental profiles we obtained for each galaxy with those presented in Mendes de Oliveira (1992), excluding the central parts,

which are usually contaminated by seeing effects, and the outer parts of the galaxy, which are affected by the sky subtraction. Even with the excluded regions, several arcseconds of the surface brightness profiles were used in the fit. The RMS of the fitting was quite small (typical RMS = 0.05 magnitudes) but realistic errors are larger (of the order of 0.1 to 0.2 magnitudes) since they depend on the reliability of the zero point for the literature data.

4 ANALYSIS AND RESULTS

4.1 Wavelet analysis

Since the IGL is an extended, very low surface brightness structure (usually less than 1% above the night sky level) many instrumental effects like flatfielding, scattered light and CCD bleeding, among others, can contaminate the signal. Therefore, very good illumination corrections and short exposure times to avoid bleeding are necessary. Besides the instrumental effects, some astronomical ones are important in this kind of analysis. The dimming of the IGL by the light from the objects in the image, like member galaxies and stars, which need to be modeled and subtracted from the image, is one major “problem” for this kind of study. Also a very accurate sky subtraction is needed for the detection and analysis of the IGL.

To deal with this kind of requirement, we applied a wavelet-based technique, the OV_WAV package (Epitácio Pereira 2003), in our analysis, as shown in Da Rocha & Mendes de Oliveira (2005). This technique does a multiscale analysis that uses the *à trous* wavelet transform, and is able to separate the structures in the image by their characteristic sizes with no *a priori* information (Bijaoui & Rue 1995; Starck et al. 1998). Since the information in astronomical images is organized hierarchically (stars projected onto galaxies, that are projected onto a larger structure like the IGL and all projected onto the sky brightness level), this technique is very well suited for our goals. This method was already applied by other authors to the same kind of study (*e.g.* Adami et al. 2005).

The main procedure is the following. The images are deconvolved into wavelet coefficients, which will contain information of a given size (2^n pixels, where n is the index of the wavelet coefficient - $n = 0, 1, 2, 3, \dots$). A source in the image, when deconvolved in wavelet coefficients, has a representation in each of the coefficients that depends on the shape and size of this object. Also the noise present in the image, has a representation in the different wavelet coefficients. The representation of the noise is analyzed and the representation of the signal is detected in each coefficient. These detections in different coefficients are interconnected, defining the detected objects and each detected object is reconstructed and separately analyzed.

The noise present in astronomical images is mostly dominated by small scale components. As the characteristic size of the wavelet coefficients increases, the representation of the noise loses intensity. With this behaviour of the noise representation, working in wavelet space, we are able to detect large structures, with very low surface brightness, with high confidence levels. Our simulations have shown that we are able to detect at a 5- σ -detection level in wavelet space, large,

¹ IRAF (Image Reduction and Analysis Facility) is distributed by the National Optical Astronomy Observatories, which is operated by the Association of Universities for Research in Astronomy, Inc., under cooperative agreement with the National Science Foundation.

low surface brightness structures, that have only $S/N = 0.1$ in real space (Da Rocha & Mendes de Oliveira 2005).

After the reconstruction of each object, in an iterative process that models and subtracts the detected sources from the image, we are able to re-compose the IGL component and the galaxies component for each group, in each band independently, and perform our analysis, which will be described below. A more detailed description of the OV_WAV and the simulations on the detection of IGL can be found in Da Rocha & Mendes de Oliveira (2005).

4.2 Group parameters

We have re-calculated the group crossing time (t_c) and mass to light ratio (M/L), previously calculated in Hickson et al. (1992), using the concordance cosmology parameters, since the original ones were calculated using $H_0 = 100 \text{ km s}^{-1} \text{ Mpc}^{-1}$ and $\Omega_M = 1.0$.

There was very small variations due to cosmology on the re-calculated values for the crossing time, which is given in unities of H_0^{-1} , since for closer groups the impact of Λ is small. On the other hand, including or excluding galaxies from the analysis, as we did for HCG 15 and HCG 51, can have a considerable effect on this value. The crossing times were calculated using the relation presented in Hickson et al. (1992)

$$t_c = \frac{4}{\pi} \frac{R}{D\sigma}. \quad (1)$$

R is the mean separation in kpc between the member galaxies and $D\sigma$ is the deprojected velocity dispersion given by

$$D\sigma = [3(\langle v^2 \rangle - \langle v \rangle^2 - \langle \sigma_v^2 \rangle)]^{1/2}, \quad (2)$$

where v is the observed recession velocity and σ_v is the measurement error.

For M/L , the total group luminosities were calculated with the member galaxies for each case and the proper distance modulus. Since X-ray mass estimates are not available for most of groups from Hickson's catalogue, and for consistent comparison, we used the same mass estimators of Hickson et al. (1992) to estimate the group's masses. The median of the four mass estimators described by Heisler, Tremaine, & Bahcall (1985) (virial mass, projected mass, median mass and mean mass) was used for each group. An important consideration should be raised here, that dynamical mass estimates using the small number of galaxies present in a compact group can suffer from severe statistical effects and should be taken only as a guiding value. These estimators only measure the mass inside the area where the galaxies are found, what corresponds only to the inner part of the detected IGL components and of the dark matter halo. Therefore, these estimators would not account for the mass in the outer parts of the group.

We have found in the literature new recession velocity measurements for some of the galaxies, as for the case of HCG 15C, which differ from the originally published values by about 30 km s^{-1} , on average. This small variation causes an impact of up to 20% in the estimated group parameters, like crossing times and masses, showing how sensitive they are to the small number of objects present in each group. For consistency we decided to use the values from Hickson et al.

(1992), unless for the case where HCG 15C is not considered a group member. Using the new recession velocities would not change the difference between the velocity of HCG 51C and the median velocity of this group.

The quantities estimated here for each group and its possible different configurations can be seen in table 3.

4.3 HCG 15

The images in B and R of HCG 15 were deconvolved into 11 wavelet coefficients (2^{10} pixels, about the size of the image), the detected objects were reconstructed in a multiple iterations process and the group galaxies and IGL component of this group were re-composed, as is shown in figure 1. The whole analysis process is made in a totally independent way for the B and R bands.

For the quintet (and sextet) configuration, the detected IGL component in this group represents $19 \pm 4\%$ ($16 \pm 3\%$) of the total light in the B band and $21 \pm 4\%$ ($18 \pm 4\%$) in the R band, about 70% of the light of the first-ranked galaxy. This component corresponds to apparent total magnitudes of $B = 15.0 \pm 0.2$ and $R = 13.3 \pm 0.2$, down to a surface brightness detection limit of $\mu_B = 31.3$ and $\mu_R = 30.5$. The detection limits correspond to a surface brightness of $0.1 \cdot \sigma_{sky}$ ($S/N = 0.1$) in each band, which is the detection limit of the OV_WAV package.

The IGL presents a very irregular shape and has a very low mean surface brightness, $\mu_B = 28.4 \pm 0.2$ and $\mu_R = 26.7 \pm 0.2$. Its mean S/N per pixel is 1.5 in B and 3.3 in R . The IGL has a mean colour $(B - R)_0 = 1.6 \pm 0.2$, redder, but still consistent with the mean colour for the galaxies' component ($(B - R)_0 = 1.4 \pm 0.2$ for the quintet configuration and $(B - R)_0 = 1.5 \pm 0.2$ for the sextet) and with the old stellar population expected from early-type galaxies. The extinction corrections were made using Rieke & Lebofsky (1985) extinction laws and Schlegel, Finkbeiner, & Davis (1998) extinction maps. The IGL and galaxy components were measured in the same areas in the two different bands. The properties of the IGL components are summarized in table 4.

The original M/L in the B band for this group, calculated by Hickson et al. (1992), was $432 \text{ M}_\odot/\text{L}_\odot$. The M/L values were converted to $H_0 = 70 \text{ km s}^{-1} \text{ Mpc}^{-1}$, while the original values were calculated with $H_0 = 100 \text{ km s}^{-1} \text{ Mpc}^{-1}$ and $\Omega_M = 1.0$. Our new estimate takes these values to 614 and $424 \text{ M}_\odot/\text{L}_\odot$, respectively for the quintet and sextet cases. Using the light contained in the IGL component, we recalculated the M/L for each of the studied groups for the new total luminosity, correcting the estimated values. In the case of HCG 15 the M/L drops to 517 and $367 \text{ M}_\odot/\text{L}_\odot$, for the two presented cases. The M/L values presented in this paper always refer to the B band.

The crossing times for this group, 0.014 H_0^{-1} (Hickson et al. 1992), had no change in both configurations, quintet and sextet. M/L and crossing time values are given in table 3.

4.4 HCG 35

As in the case of HCG 15, the B and R images of HCG 35 were deconvolved into 11 wavelet coefficients and the galaxies and IGL component were re-composed after the wavelet

Table 3. Group parameters for each configuration.

	HCG 15 (5G)	HCG 15 (6G)	HCG 35	HCG 51 (5G)	HCG 51 (6G)
$D\sigma$ (km s ⁻¹)	726.9	730.0	547.8	409.4	844.9
t_c (H ₀ ⁻¹)	0.014	0.014	0.011	0.019	0.009
M/L (M _⊙ /L _⊙)	614	424	55	50	174
M/L corrected (M _⊙ /L _⊙)	517	367	48	38	139
Group Mass (M _⊙)	5.67·10 ¹³	5.30·10 ¹³	1.51·10 ¹³	7.39·10 ¹²	3.59·10 ¹³
E-type fraction	0.4	0.5	0.8	0.6	0.7

5G and 6G designations corresponds to quintet and sextet configurations of HCG 15 and HCG 51.

Figure 1. IGL component of HCG 15 identified and reconstructed with the OV_WAV package. The left panel shows the image in the B band and the IGL component as contour curves with surface brightness levels which range from 27.0 to 31.0 magnitudes in steps of 0.25 B mag arcsec⁻², from the inner to the outer part. The right panel shows the image in the R band and the IGL component as contour curves with surface brightness levels which range from 25.5 to 29.0 magnitudes in steps of 0.25 R mag arcsec⁻², from the inner to the outer part.

multiple iteration process, as can be seen in figure 2, where the analysis of the B and R bands are independent.

In this group the detected IGL component presents an irregular shape, elongated in the same direction as the galaxy component elongation. This component represents $15 \pm 3\%$ of the total light in the B band and $11 \pm 2\%$ in the R band, 40% of the light of the first-ranked galaxy. The total apparent magnitudes of the IGL are 16.4 ± 0.2 and 14.9 ± 0.2 , respectively in the B and R bands, down to a surface brightness detection limit of $\mu_B = 31.0$ and $\mu_R = 28.8$.

This group presents quite a faint IGL component with a mean surface brightness of $\mu_B = 27.9 \pm 0.2$ and $\mu_R = 26.4 \pm 0.2$. The mean S/N per pixel of the IGL is 1.7 in B and 1.0 in R . Its mean colour is $(B-R)_0 = 1.5 \pm 0.2$ and the galaxies have a mean $(B-R)_0 = 1.8 \pm 0.2$. In this case the IGL component is bluer than the mean colour for the galaxies, but consistent with the typical colour for old stellar population in early-type galaxies, while the galaxy’s component is redder than the typical value for early-type galaxies. The mean colour measured for the galaxies’ component is not surprising considering that, at least 3 galaxies present colours measured inside the $\mu_R = 24.5$ isophote around $(B-R)_0 = 1.9$, including one Sb galaxy (Hickson, Kindl, & Auman 1989). IGL properties are shown in table 4.

The new estimate of the M/L in the B band takes the value from 57 (Hickson et al. 1992, converted to $H_0 = 70$ km s⁻¹ Mpc⁻¹) to 55 M_⊙/L_⊙. Correcting it by the light in the IGL, the M/L drops to 48 M_⊙/L_⊙. t_c slightly increased from 0.010 (Hickson et al. 1992) to 0.011 H₀⁻¹. The re-estimated parameters for this group can be seen in table 3.

4.5 HCG 51

This group’s images were analyzed in the same way as the previous two and the IGL component can be seen in figure 3.

This group presents a more prominent elliptical shape in the IGL component, following the elongation of the galaxies distribution with some clear tidal features. The IGL, in the quintet (and sextet) configuration, represents $31 \pm 6\%$ ($26 \pm 5\%$) and $28 \pm 5\%$ ($24 \pm 5\%$) of the total light in the B and R bands, respectively, about 70% of the light of the first-ranked galaxy. This corresponds to apparent total magnitudes of

Figure 4. Image of HCG 51 in the B band showing the jet-like structure (marked with the white ellipse) connecting HCG 51A and 51E.

$B = 14.4 \pm 0.2$ and $R = 12.9 \pm 0.2$, down to the limiting surface brightnesses of $\mu_B = 30.7$ and $\mu_R = 29.7$.

The mean surface brightness of this component is $\mu_B = 27.4 \pm 0.2$ and $\mu_R = 25.9 \pm 0.2$. The mean S/N is 2.0 in B and 3.4 in R . The IGL has a mean colour $(B-R)_0 = 1.5 \pm 0.2$, about the same as the mean colour of the galaxies, $(B-R)_0 = 1.6 \pm 0.2$ for both configurations, as expected for early-type galaxies with old stellar population. The properties of the IGL component can be seen in table 4.

The new estimate of the M/L in the B band was performed for this group, that goes from 51 (Hickson et al. 1992, converted to $H_0 = 70$ km s⁻¹ Mpc⁻¹) to 50 and 174 M_⊙/L_⊙, for quintet and sextet configurations. It drops to 38 and 139 M_⊙/L_⊙, when corrected for the diffuse component contribution.

The crossing time of this group, originally 0.019 H₀⁻¹, presented no change for the quintet configuration and drastically drops to 0.009 H₀⁻¹, for the sextet configuration. The large difference between the M/L and the crossing time, for the quintet and sextet configuration, is due to the deprojected velocity dispersion that is twice as large in the latter case, what can also be noticed in the 2-D velocity dispersion (tables 1 and 3).

In HCG 51 we detected a very low surface brightness jet-like structure that connects galaxies HCG 51A and 51E. This structure is redder than the mean colour of the galaxy’s component and of the IGL ($(B-R)_0 = 1.8 \pm 0.2$) and has a mean surface brightness $\mu_B = 27.0 \pm 0.2$ and $\mu_R = 25.2 \pm 0.2$. The estimated extension of this structure is 90 kpc, about the mean galaxy separation, actually this structure connects the two “parts” of this group. The images also show a possible shell-like structure perpendicular to the jet-like one, but it is too faint and small to be detected as an independent object and properly analyzed. This jet-like structure can be seen in figure 4. No further tidal structures were detected in this group.

Figure 2. IGL component of HCG 35 identified and reconstructed with the OV_WAV package. The left panel shows the image in the B band and the IGL component as contour curves with surface brightness levels which range from 27.5 to 29.0 magnitudes in steps of $0.25 \text{ B mag arcsec}^{-2}$, from the inner to the outer part. The right panel shows the image in the R band and the IGL component as contour curves with surface brightness levels which range from 25.75 to 27.5 magnitudes in steps of $0.25 \text{ R mag arcsec}^{-2}$, from the inner to the outer part.

Figure 3. IGL component of HCG 51 identified and reconstructed with the OV_WAV package. The left panel shows the image in the B band and the IGL component as contour curves with surface brightness levels which range from 26.5 to 29.0 magnitudes in steps of $0.25 \text{ B mag arcsec}^{-2}$, from the inner to the outer part. The right panel shows the image in the R band and the IGL component as contour curves with surface brightness levels which range from 24.75 to 27.5 magnitudes in steps of $0.25 \text{ R mag arcsec}^{-2}$, from the inner to the outer part.

4.6 Structural Analysis of the IGL

As can be seen in figures 1 to 3, the IGL components detected in our study clearly show very irregular shapes, in contrast with the ICL components detected in clusters of galaxies (e.g. Krick & Bernstein 2007).

In order to quantify how regular, or irregular, the light distribution can be, we perform the modeling of the IGL component using elliptical isophotes with the IRAF package STSDAS.ELLIPSE. This analysis leaves large residuals when the elliptical models are subtracted from the IGL, even in the case of HCG 51 that shows an apparently less irregular IGL component. These large residuals are already an indication of the lack of regularity of the IGL distribution.

To understand the physical meaning of the fitted elliptical models, we plotted the surface brightness profiles along the major axis, which presented a multimodal behavior in all the cases. We tried to fit four types of light profiles to our data: Exponential, de Vaucouleurs, King-like core model and Hubble-Reynolds, that should work as an analytic proxy for a NFW universal profile (Navarro, Frenk, & White 1997), as suggested by Lokas & Mamon (2001) and Krick & Bernstein (2007). The profile fitting, in all cases, either single or double component, led to unphysical results for parameters as effective radius or scale length (being extremely small or extremely large), for example, indicating no dynamical equilibrium.

The unphysical results obtained by the fits, show that the elliptical models do not represent any physical entity, as expected considering the large residuals when these models are subtracted. The failure on fitting the surface brightness profiles is another indication that the IGL components are very irregular and cannot be described by a regular model, as it happens in the diffuse component of clusters of galaxies. We can conclude from this, already, that the compact groups are far from being a relaxed and virialized structure.

The analysis of the colour maps of the reconstructed IGL components of all groups do not show any kind of substructures, such as blue regions that could be associated to star forming regions in the IGL. Blue star forming regions in the diffuse component, as found in the Coma cluster by Adami et al. (2005), could be the origin of the difference we find between the mean colour of the IGL and the one of the galaxy component, when the IGL is bluer than the galaxies. In the case of our study, those regions, if they exist, could be too disperse to be individually identified in our colour maps.

4.7 Dynamical Evolution Indicators

Some group properties can be used as dynamical evolution indicators, such as fraction of early-type galaxies (or of late-type galaxies), crossing time and magnitude difference between the first and the second-ranked galaxies (Δm_{12}). Now we have an additional dynamical evolution indicator, the fraction of IGL present in the group.

In a first qualitative effort, we analyzed the relation between these indicators in our sample. We restricted this analysis to the groups studied here and in Da Rocha & Mendes de Oliveira (2005) in order to have a homogeneously analyzed sample and the analysis is only qualitative due to small number of objects, only 6 groups.

We can see the relations between the fraction of IGL in the B band (F_{IGL}), the fraction of early-type galaxies (F_{Egal}), the crossing time (t_{cross}) and Δm_{12} , in figure 5. The fractions of IGL in the B and R band are very similar, and for this kind of study do not present any difference in the relation with the other indicators.

HCG 15 and 51 are presented with two data points each, for the quintet and sextet configurations. For HCG 88 we have found new recession velocity measurements (Nishiura et al. 2000b). The new measurements increase the velocity dispersion of the group from 31 to 93 km s^{-1} , allowing the estimate of the deprojected velocity dispersion (134 km s^{-1}) and reducing the crossing time from 8.7 to 0.065 H_0^{-1} , therefore we included a “new point” for this group in the relations between t_{cross} and other quantities. This decrease in the crossing time do not alter the conclusions about this object given in Da Rocha & Mendes de Oliveira (2005), since the value is still considerably high.

The relations with Δm_{12} show no clear tendency. Relations between F_{IGL} , F_{Egal} and t_{cross} can be, in a first approximation, described in a linear relation, if the clearly discrepant objects are excluded. We excluded the “old” high t_{cross} value of HCG 88 from the fits for relations with this quantity and HCG 35, that shows a very high fraction of early-type galaxies, was excluded from the fits for relations with F_{Egal} . These relations show the agreement, in a qualitative way, between our new dynamical evolution indicator, the fraction of the total light in the IGL and the fraction of early-type galaxies and the group crossing time.

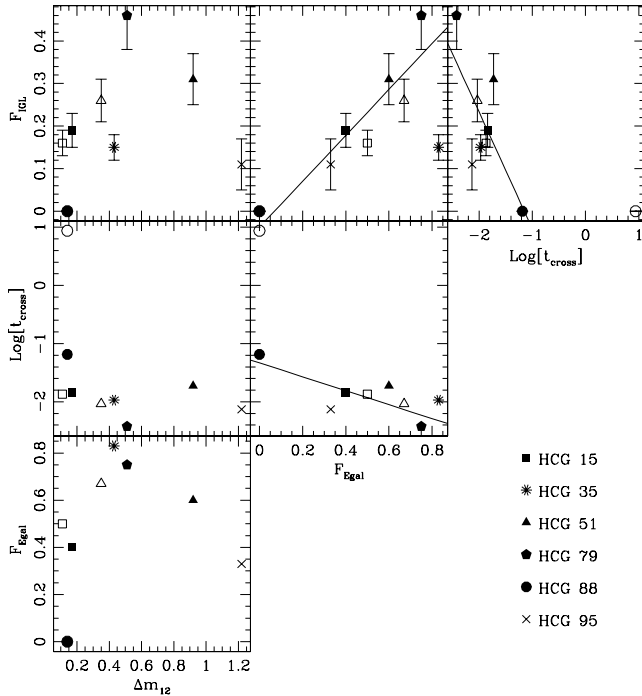
Table 4. Properties of the IGL component detected in our sample.

Group	% (<i>B</i> and <i>R</i>)		μ (<i>B</i> and <i>R</i>)		Mag. (<i>B</i> and <i>R</i>)		(<i>B</i> − <i>R</i>) ₀
HCG 15	19 ± 4% / 16 ± 3%	21 ± 4% / 18 ± 4%	28.4 ± 0.2	26.7 ± 0.2	15.0 ± 0.2	13.3 ± 0.2	1.6 ± 0.2
HCG 35	15 ± 3%	11 ± 2%	27.9 ± 0.2	26.4 ± 0.2	16.4 ± 0.2	14.9 ± 0.2	1.5 ± 0.2
HCG 51	31 ± 6% / 26 ± 5%	28 ± 5% / 24 ± 5%	27.4 ± 0.2	25.9 ± 0.2	14.4 ± 0.2	12.9 ± 0.2	1.5 ± 0.2

Column (1) Group studied.

Columns (2-3) Fraction of the group’s total light in the IGL component, bands *B* and *R*, respectively (the values presented for HCG 15 and 51 are for the quintet and sextet configurations)Columns (4-5) Mean surface brightness of the IGL component, bands *B* and *R*, respectively.Columns (6-7) Integrated magnitude of the IGL component, bands *B* and *R*, respectively.

Column (8) Extinction corrected colour of the IGL component.

**Figure 5.** Relations between different dynamical evolution indicators (F_{IGL} , F_{Egal} , t_{cross} and Δm_{12}). The continuous lines are linear fits to the points, excluding the ones that clearly deviate from the main trend. The quintet configurations for HCG 15 and HCG 51 are shown with filled symbols and the sextet configurations are shown with the corresponding open symbol. The “new” crossing time value for HCG 88 is shown in filled symbol, while the “old” value is shown in open symbol.

5 DISCUSSION AND CONCLUSIONS

Before we start the discussion, we present a short summary of the results of this work:

(1) We applied our wavelet analysis technique (the OV_WAV package) to study the IGL component in 3 further compact groups of galaxies, completing a sample of 6 objects studied with this technique.

(2) HCG 15 had to be analyzed in two configurations (quintet and sextet) and we were able to detect an IGL component that corresponds to $19 \pm 4\% / 16 \pm 3\%$ of the total light in the *B* band and $21 \pm 4\% / 18 \pm 4\%$ in the *R* band. The mean colour of the IGL is $(B - R)_0 = 1.6 \pm 0.2$ consistent with the galaxies’ mean colour.

(3) HCG 35 has IGL components which represent fractions of $15 \pm 3\%$ and $11 \pm 3\%$ of the total light in the *B* and *R* bands, respectively, with a mean colour $(B - R)_0 = 1.5 \pm 0.2$, bluer than the mean colour of the galaxy component.

(4) HCG 51, which also had to be analyzed in two configurations (quintet and sextet), presented $31 \pm 6\% / 26 \pm 5\%$ and $28 \pm 5\% / 24 \pm 5\%$ of the total light in bands *B* and *R* in the IGL component. The mean colour of the IGL component $(B - R)_0 = 1.5 \pm 0.2$ is compatible with the galaxy component mean colour.

(5) All the objects of this sample present irregular IGL components. The analysis was made independently in the *B* and *R* bands and the shape of the detected components agree in both bands, showing the reliability of the method.

(6) We find that the fraction of intragroup light, in the groups studied so far, correlates, in a qualitative way, with other indicators of dynamical evolution, such as the fraction of early-type galaxies in the group and the crossing times.

As we already showed in Da Rocha & Mendes de Oliveira (2005), using the wavelet technique OV_WAV, we can detect the intragroup component present in compact groups of galaxies in a very reliable way and without any “a priori” information or assumptions about properties of the member galaxies or of the image.

The components we detect correspond to about 40 to 75% of the luminosity of group first-ranked galaxies, which is equivalent to 15 to 35% of a typical M_* luminosity ($M_B = -21.9$ Hunsberger, Charlton, & Zaritsky 1998), where the first-ranked galaxies of the three studied objects have magnitudes fainter than M_* . The fraction of light in the IGL can be used as a measure of the amount of interaction suffered by the member galaxies, which is expected to be proportional to the number of crossings the galaxies suffered since the group formation. By relating the amount of light in the IGL with the expected amount of stripped matter in each crossing we can estimate how many times the galaxy crossed the group. The missing link here is the amount of matter stripped on average in each crossing, which is sensitive to the distribution of the dark matter and requires numerical simulations with very realistic initial conditions to be determined.

The colours of the IGL are compatible with the colours of the galaxy component. In general this would indicate that the striping is due to ongoing interactions, while redder colours for the IGL would indicate an older stripping, since the stripped stars would evolve passively and the galaxy would keep forming stars and maintaining a bluer colour. In the case of compact groups, specially the ones studied

here, this relation can be misleading, since in these early-type dominated groups, the galaxies do not typically have star formation.

In the cases of HCG 35 and 51, the IGL is bluer than the mean colour of the galaxy component, but still in agreement with each other. The colours could indicate that some star formation regions were or are being stripped from the galaxies, or that some star formation could be occurring “in situ”. As the groups have mostly early-type galaxies, no star formation seems to be occurring there, even though interactions are effectively happening, as can be noticed by the presence of a red jet-like and probably also a very faint shell-like structure in HCG 51. As in the case of HCG 79 (Da Rocha & Mendes de Oliveira 2005), where the colour difference was much larger than here, the cause for this difference can also be the destruction of dwarf galaxies.

In the case of HCG 15, the IGL component is redder than the mean colour of the galaxies’ component, but also still in agreement, and the fraction of early-type galaxies is lower. This could be the case of stripped stars evolving passively, while the galaxies keep forming stars. In this group also no signs of strong star formation can be seen.

Ongoing interactions that do not form new stars, lead us to the conclusion that the evolution of compact groups would be closely related to the scenario of “dry mergers”. In the dry mergers scenario (van Dokkum 2005) most of the luminous field elliptical galaxies are assembled not via high redshift gas rich disks, galaxy mergers or monolithic collapse, but via merger of gas poor, bulge dominated objects.

The shapes of the detected IGL components are very irregular (see figures 1 to 3) and cannot be described with elliptical isophotes leading to large residuals. Also, the fitted surface brightness profiles, lead to unphysical parameters for the fit profiles (exponential, de Vaucouleurs, King-like core model and Hubble-Reynolds), show that this component is irregular in its whole extent.

The group’s gravitational potential is dominated by the group’s dark matter halo and we assume that the light traces the mass. If the IGL is due to stripped stars that are distributed following the group’s dark matter dominated potential, the irregular shape of the IGL lets us conclude that the groups are definitely not virialized structures. They would be in a compact configurations for long enough to have part of the stars stripped from the galaxies and dispersed in the group potential, but not enough to get in equilibrium.

The non-equilibrium situation, together with the small number of galaxies, makes the estimate of group dynamical parameters, such as mass and crossing time, very uncertain and sensitive to small variations of the input data, as mentioned in section 4.2.

An important parameter is the total mass of the group, which can only be determined dynamically, using the member galaxies, due to the inexistence of other determinations, such as through X-ray observations. In the case of compact groups of galaxies, the dynamical mass estimators can only be used as an indicator, since the structure, as we showed before, is not virialized. Also, they are only sensitive to the mass inside the area occupied by the galaxies (the “galaxies circle”), which in the case of a compact group, can leave a considerable part of the mass unaccounted for.

McConnachie, Ellison, & Patton (2008) studied the properties of compact groups of galaxies identified in a mock

galaxy catalogue based on the Millennium Run simulation (Springel et al. 2005). These authors found that the member galaxies are in the inner part of the common dark matter halo of the group and that there is no correlation between the halo virial radius and how the galaxies are concentrated towards the center of the group.

We could approach this question in two extreme ways. One is assuming that the dark matter halo dominates the mass in the whole extent of the group and that the galaxies do not contribute significantly to it. In this case the dark matter mass could be directly related to the IGL luminosity, so that the fraction of mass unaccounted would be proportional to the fraction of IGL outside the “galaxies circle”. The missing fraction, in this case, would be about 60 to 70% of the total mass. The second approach is to assume that the galaxies dominate the mass in the inner part of the group and that we have a constant M/L in the whole structure. In this case the missing fraction would not be larger than 10% of the total mass.

We are not able to pin down a number for the unaccounted mass, as we are not able to pin down a number for the total mass itself using dynamical estimators. The non-equilibrium state of the compact groups, together with the fraction of the total mass that can be measured by dynamical mass indicators, prevent us from a reliable mass determination. Other mass estimators, as X-rays, assume that the structure is in equilibrium, what can lead to the same kind of uncertainties. For lensing estimates the small distance of the groups and their low masses turn the detection of the shear signal, if possible, very complicated. A recent work on the Coma cluster (Kubo et al. 2007), which is about the same distance as most of the HCGs, determined its mass using weak lensing detected with deep, large field of view, images from the SDSS. Even though the distances are similar, the difference in total mass between Coma and the HCGs, would still be a problem for detecting the shear signal. According to Mendes de Oliveira & Giraud (1994), the HCGs would need a distance 10 times larger to produce a detectable lensing signal.

In a qualitative way (our sample is too small for a more quantitative result), we could show that the fraction of IGL agrees with other dynamical evolution indicators such as the fraction of early-type galaxies and the crossing time. The crossing time, as the mass, is sensitive to small variations on the input parameters, as we showed for the case of the previously studied group HCG 88. We can also see that the magnitude difference between the first and the second-ranked galaxies does not clearly correlate with any of the other indicators. Hickson et al. (1992) shows that the crossing time correlates with the fraction of spirals (complementary to the fraction of early-type galaxies) and Δm_{12} (figures 5 and 6 in their paper), but for objects in bins of crossing time. The correlation using individual objects was not shown. So the correlation of Δm_{12} , on average, could eventually be seen when we have a considerably larger sample.

The new discordant velocity of HCG 15C, which has a much larger radial velocity (by 2720 km s^{-1}) than the median velocity of the group, is a point to be considered with care. Galaxies in HCGs are bright enough for a good recession velocity determination and both sources, the UZC and Hickson et al. (1992), have reliable redshift determinations.

Altering the original group configuration, as excluding

HCG 15C (due to its new published recession velocity) or including HCG 51C (extending the definition of “discordant velocity”) puts a challenge on defining which is the “correct” configuration for each of the groups. In figure 5 we can see the location of each of the two configurations for both systems. For HCG 15, the relation between F_{Egal} and t_{cross} leaves all the points too close to the line for any consideration, as so does the relation between t_{cross} and F_{IGL} , but in the relation between F_{Egal} and F_{IGL} , the quintet configuration shows a better agreement with the main trend of the dynamical evolution indicators. In the case of HCG 51, the relation between F_{Egal} and t_{cross} and between t_{cross} and F_{IGL} would favor the sextet configuration, while the relation between F_{Egal} and F_{IGL} , would favor the quintet one.

Of course this kind of “selection” is very speculative, since both configurations mostly agree between the errors. In a possible more quantitative analysis, we can be able to extrapolated this kind of relation as a test to verify if a galaxy that has an accordant redshift, but do not seem to be involved in the interactions occurring in the group, is a member of the group in a dynamical sense.

We can update our evolutionary sequence envisioned in Da Rocha & Mendes de Oliveira (2005), where we placed HCG 79 in the advanced stage of dynamical evolution, HCG 95 in the intermediary stage and HCG 88 in the initial stage. The three groups presented here would be placed in the intermediary stage. All the objects have fraction of IGL between 10 and 30% (with the exception of HCG 51, when the quintet configuration is considered it has 31% of IGL fraction), the crossing times are in the “middle region” (not as long as HCG 88 and not as short as HCG 79) and the fraction of early-type galaxies is around 0.5 (except for HCG 35 that has 0.83, clearly disagreeing with the other indicators for this same group).

The fraction of early-type galaxies of HCG 35 is in clear disagreement with the other indicators of dynamical evolution. This group also shows an overabundance of HI, when compared to the expected HI content of the group (estimated by the morphological type and luminosity of its member galaxies). Its HI content is about 29% higher than the expected, while HCG 15 and 51, in the configurations published in Hickson et al. (1992), are HI deficient (about 70% of the expected HI is missing). However, the HI content of this group is dominated by the one Sb member galaxy (all the other 5 members are early-type galaxies, where almost no HI is expected) and the HI content of an Sb galaxy can vary by a factor of 3, higher or lower than the typical value (Roberts & Haynes 1994). This shows that this group needs some extra attention and studies.

The detection and analysis of IGL component in compact groups is feasible and efficient, the results can be used as a dynamical evolution indicator and can provide initial conditions to numerical simulations in the search for a better understanding of group formation and evolution and also to the formation and evolution of clusters of galaxies.

Based on observations collected at the Centro Astronómico Hispano Alemán (CAHA) at Calar Alto, operated jointly by the Max-Planck Institut für Astronomie and the Instituto de Astrofísica de Andalucía (CSIC). We would like to thank Carlos Rabaça and Daniel Epitácio Pereira for the software development and support and Hugo Capelato for

discussions and support to this project. We thank the support from the Deutsches Zentrum für Luft- und Raumfahrt, DLR (project number 50 OR 0602), Deutsche Forschungsgemeinschaft, DFG (project number ZI 663/8–1) within the Priority Program 1177 (SPP/DFG), Volkswagen Foundation (project number I/76 520) and Fundação de Amparo a Pesquisa do Estado de São Paulo, FAPESP (Project number 02/06881–4). CMdO would like to acknowledge support from the Brazilian agencies FAPESP (projeto temático 01/07342–7), CNPq and CAPES. We would like to thank the anonymous referee for the useful comments that considerably improved this manuscript.

REFERENCES

- Adami C., Slezak E., Durret F., Conselice C. J., Cuillandre J. C., Gallagher J. S., Mazure A., Pelló R., Picat J. P., Ulmer M. P., 2005, *A&A*, 429, 39
- Bijaoui A., Rue F., 1995, *Signal Processing*, 46, 345
- Conroy C., Wechsler R. H., Kravtsov A. V., 2007, *ApJ*, 668, 826
- Covone G., Adami C., Durret F., Kneib J.-P., Lima Neto G. B., Slezak E., 2006, *A&A*, 460, 381
- Da Rocha C., Mendes de Oliveira C., 2005, *MNRAS*, 364, 1069
- Danese L., de Zotti G., di Tullio G., 1980, *A&A*, 82, 322
- Dressler A., 1984, *ARA&A*, 22, 185
- Epitácio Pereira D. N., 2003, *A Transformada de Wavelet Aplicada a Imagens Astronômicas*. Undergraduate Thesis
- Falco E. E., Kurtz M. J., Geller M. J., Huchra J. P., Peters J., Berlind P., Mink D. J., Tokarz S. P., Elwell B., 1999, *PASP*, 111, 438
- Gonzalez A. H., Zaritsky D., Zabludoff A. I., 2007, *ApJ*, 666, 147
- Heisler J., Tremaine S., Bahcall J. N., 1985, *ApJ*, 298, 8
- Hickson P., 1982, *ApJ*, 255, 382
- Hickson P., Kindl E., Auman J. R., 1989, *ApJS*, 70, 687
- Hickson P., Mendes de Oliveira C., Huchra J. P., Palumbo G. G., 1992, *ApJ*, 399, 353
- Hunsberger S. D., Charlton J. C., Zaritsky D., 1998, *ApJ*, 505, 536
- Jones L. R., Ponman T. J., Horton A., Babul A., Ebeling H., Burke D. J., 2003, *MNRAS*, 343, 627
- Krick J. E., Bernstein R. A., 2007, *AJ*, 134, 466
- Kubo J. M., Stebbins A., Annis J., Dell’Antonio I. P., Lin H., Khiabanian H., Frieman J. A., 2007, *ApJ*, 671, 1466
- Lokas E. L., Mamon G. A., 2001, *MNRAS*, 321, 155
- McConnachie A. W., Ellison S. L., Patton D. R., 2008, *ArXiv e-prints*, 0804, 2928
- Mendes de Oliveira C., 1992, PhD thesis, The University of British Columbia (Canada).
- Mendes de Oliveira C., Giraud E., 1994, *ApJ*, 437, L103
- Mendes de Oliveira C., Hickson P., 1994, *ApJ*, 427, 684
- Mihos J. C., 2004, in *Clusters of Galaxies: Probes of Cosmological Structure and Galaxy Evolution*, Mulchaey J. S., Dressler A., Oemler A., eds., p. 277
- Moles M., Marquez I., Sulentic J. W., 1998, *A&A*, 334, 473
- Monaco P., Murante G., Borgani S., Fontanot F., 2006, *ApJ*, 652, L89
- Mulchaey J. S., Davis D. S., Mushotzky R. F., Burstein D., 2003, *ApJS*, 145, 39

- Murante G., Arnaboldi M., Gerhard O., Borgani S., Cheng L. M., Diaferio A., Dolag K., Moscardini L., Tormen G., Tornatore L., Tozzi P., 2004, *ApJ*, 607, L83
- Murante G., Giovalli M., Gerhard O., Arnaboldi M., Borgani S., Dolag K., 2007, *MNRAS*, 377, 2
- Navarro J. F., Frenk C. S., White S. D. M., 1997, *ApJ*, 490, 493
- Nishiura S., Murayama T., Shimada M., Sato Y., Nagao T., Molikawa K., Taniguchi Y., Sanders D. B., 2000a, *AJ*, 120, 2355
- Nishiura S., Shimada M., Ohyama Y., Murayama T., Taniguchi Y., 2000b, *AJ*, 120, 1691
- Osmond J. P. F., Ponman T. J., 2004, *MNRAS*, 350, 1511
- Pildis R. A., Bregman J. N., Schombert J. M., 1995, *AJ*, 110, 1498
- Ponman T. J., Allan D. J., Jones L. R., Merrifield M., McHardy I. M., Lehto H. J., Luppino G. A., 1994, *Nature*, 369, 462
- Ponman T. J., Bournier P. D. J., Ebeling H., Bohringer H., 1996, *MNRAS*, 283, 690
- Purcell C. W., Bullock J. S., Zentner A. R., 2007, *ApJ*, 666, 20
- Rieke G. H., Lebofsky M. J., 1985, *ApJ*, 288, 618
- Roberts M. S., Haynes M. P., 1994, *ARA&A*, 32, 115
- Rose J. A., 1979, *ApJ*, 231, 10
- Rudick C. S., Mihos J. C., McBride C., 2006, *ApJ*, 648, 936
- Schlegel D. J., Finkbeiner D. P., Davis M., 1998, *ApJ*, 500, 525
- Seigar M. S., Graham A. W., Jerjen H., 2007, *MNRAS*, 378, 1575
- Sommer-Larsen J., 2006, *MNRAS*, 369, 958
- Springel V., White S. D. M., Jenkins A., Frenk C. S., Yoshida N., Gao L., Navarro J., Thacker R., Croton D., Helly J., Peacock J. A., Cole S., Thomas P., Couchman H., Evrard A., Colberg J., Pearce F., 2005, *Nature*, 435, 629
- Starck J.-L., Murtagh F., Bijaoui A., 1998, *Image processing and data analysis. The multiscale approach*. Cambridge, UK: Cambridge University Press, iSBN: 0521590841
- Sulentic J. W., Lorre J. J., 1983, *A&A*, 120, 36
- van Dokkum P. G., 2005, *AJ*, 130, 2647
- Verdes-Montenegro L., Yun M. S., Williams B. A., Huchtmeier W. K., Del Olmo A., Perea J., 2001, *A&A*, 377, 812
- Vílchez-Gómez R., 1999, in *Astronomical Society of the Pacific Conference Series*, Vol. 170, *The Low Surface Brightness Universe*, Davies J. I., Impey C., Phillips S., eds., p. 349
- White P. M., Bothun G., Guerrero M. A., West M. J., Barkhouse W. A., 2003, *ApJ*, 585, 739
- Zibetti S., 2007, in *IAU Symposium*, Vol. 244, *IAU Symposium*, pp. 176–185
- Zibetti S., White S. D. M., Schneider D. P., Brinkmann J., 2005, *MNRAS*, 358, 949
- Zwicky F., 1951, *PASP*, 63, 61

This figure "DaRocha.fig01a.jpg" is available in "jpg" format from:

<http://arxiv.org/ps/0805.4015v2>

This figure "DaRocha.fig01b.jpg" is available in "jpg" format from:

<http://arxiv.org/ps/0805.4015v2>

This figure "DaRocha.fig02a.jpg" is available in "jpg" format from:

<http://arxiv.org/ps/0805.4015v2>

This figure "DaRocha.fig02b.jpg" is available in "jpg" format from:

<http://arxiv.org/ps/0805.4015v2>

This figure "DaRocha.fig03a.jpg" is available in "jpg" format from:

<http://arxiv.org/ps/0805.4015v2>

This figure "DaRocha.fig03b.jpg" is available in "jpg" format from:

<http://arxiv.org/ps/0805.4015v2>

This figure "DaRocha.fig04.jpg" is available in "jpg" format from:

<http://arxiv.org/ps/0805.4015v2>